Structure and interactions in fluids of prolate colloidal ellipsoids: Comparison between experiment, theory, and simulation

A. P. Cohen,[1] E. Janai,[1] D. C. Rapaport,[2] A. B. Schofield,[3] and E. Sloutskin[1,a)]

[1]*Physics Department and Institute for Nanotechnology and Advanced Materials, Bar-Ilan University, Ramat-Gan 52900, Israel*
[2]*Department of Physics, Bar-Ilan University, Ramat-Gan 52900, Israel*
[3]*The School of Physics and Astronomy, University of Edinburgh, Edinburgh EH9 3JZ, United Kingdom*

The microscopic structure of fluids of simple spheres is well known. However, the constituents of most real-life fluids are non-spherical, leading to a coupling between the rotational and translational degrees of freedom. The structure of simple dense fluids of spheroids – ellipsoids of revolution – was only recently determined by direct experimental techniques [A. P. Cohen, E. Janai, E. Mogilko, A. B. Schofield, and E. Sloutskin, Phys. Rev. Lett. **107**, 238301 (2011)]. Using confocal microscopy, it was demonstrated that the structure of these simple fluids cannot be described by hard particle models based on the widely used Percus-Yevick approximation. In this paper, we describe a new protocol for determining the shape of the experimental spheroids, which allows us to expand our previous microscopy measurements of these fluids. To avoid the approximations in the theoretical approach, we have also used molecular dynamics simulations to reproduce the experimental radial distribution functions $g(r)$ and estimate the contribution of charge effects to the interactions. Accounting for these charge effects within the Percus-Yevick framework leads to similar agreement with the experiment. © *2012 American Institute of Physics.* [http://dx.doi.org/10.1063/1.4765100]

I. INTRODUCTION

A fluid of spheroids – ellipsoids of revolution – is among the simplest and most fundamental models of disordered matter, where positional and rotational degrees of freedom of the constituent particles are coupled. However, while fluids of highly anisometric rods[2–7] and systems of spherical particles[8–11] have been intensively studied, with the result that their structure is reasonably well understood, the structure of a dense fluid of simple spheroids was only recently determined by direct experimental measurements,[1] and a full theoretical understanding of the observed structures has not yet been attained.

Colloids – micron-sized particles suspended in a molecular solvent – are common in food industry, cosmetics, and pharmaceutics.[12] In addition, colloids are also considered a simple model to mimic systems of atoms and molecules. Since they are observable with confocal microscopy, colloids provide insight into the behavior of many-body systems, making it possible to resolve each individual particle in real motion, in three spatial dimensions.[8–10,13] Thus, these systems constitute a unique source of experimental information, forming a bridge between the behavior of individual particles and macroscopic thermodynamics.[14]

During the last decade, significant progress has been made in the synthesis of fluorescent colloids[15] with better protocols being established,[16] allowing for the formation of more stable suspensions. Simultaneously, the image processing techniques used to examine these systems evolved,[17–19] permitting higher quantity and quality of data to be collected and analyzed.[13] This progress was exploited in many experiments, where real-time three-dimensional (3D) confocal microscopy was employed to collect highly detailed information on systems of spherical colloids.[8–10,13,20] Considerably less attention has been devoted to systems of *non-spherical* colloids, such as ellipsoids.[21–26] While a few microscopy studies of thermodynamically equilibrated[27] and out-of-equilibrium two-[23] and three-dimensional[21,22,28] systems of ellipsoids have been carried out, our very recent short publication[1] is hitherto the only work to measure the microscopic structure of a 3D fluid of simple ellipsoids by direct confocal microscopy.

The current work provides a full account of our confocal measurements[1] of radial distribution functions $g(r)$ in colloidal suspensions of prolate ellipsoids, with an aspect ratio of $t = 1.6$. We introduce a new protocol, based on scanning electron microscopy, which allows the aspect ratio distribution of our ellipsoidal colloids[21,24] to be fully characterized. We also perform molecular dynamics simulations,[29] employing particles that closely approximate the shape of the experimental ellipsoids. The molecular dynamics results must be rescaled to reproduce the experimental $g(R)$, in a manner consistent with the presence of charges in the suspension. While the original Percus-Yevick theory[30] does not fit the experimental $g(R)$, similar rescaling leads to a corresponding improvement in the fit to experiment.

II. EXPERIMENTAL DETAILS

A. Formation of colloidal ellipsoids

We form ellipsoids by uniaxial stretching of simple colloidal spheres, following the procedure[31,32] which was used

---

a)Electronic mail: eli.sloutskin@biu.ac.il.

in the past with polystyrene[33] and poly(methyl methacrylate) (PMMA) particles stabilized by a grafted layer of PMMA-g-PDMS [poly(dimethylsiloxane)] copolymer.[21,22] Our initial spherical colloids are made of PMMA and coated by a sterically stabilizing layer of polyhydroxystearic acid (PHSA). The thickness of the PHSA monolayer[34] is below 10 nm, such that the interparticle potential between the initial (unstreched) colloidal spheres is closely approximated by the hard sphere model.[34,35] The reason for choosing PMMA, rather than polystyrene[33] or inorganic materials,[4,7,36] is that the density and the refractive index of PMMA can be matched by mixtures of common organic solvents to form stable suspensions, where light scattering is minimized for confocal imaging deep into the bulk of the sample. The initial spheres are fluorescently labelled by the Nile Red dye, for confocal measurements. The average diameter of the initial spheres is $\sigma_s = 2.40 \pm 0.04$ μm, as determined by static and dynamic light scattering techniques. The polydispersity of the initial spheres is below 4%, as demonstrated by the scanning electron microscopy (SEM) image in Fig. 1(a). This polydispersity is below the detection limit of conventional dynamic light scattering techniques.[37] The technical details of the stretching procedure are described in the Appendix.

B. Shape characterization

To characterize the shape of colloidal particles, we deposit them from hexane onto a clean aluminum substrate and obtain SEM images at 30 keV, employing the Quanta Inspect (*FEI^{TM}*) electron microscopy setup. A typical image of our initial spherical particles is shown in Fig. 1(a). The ellipsoids,
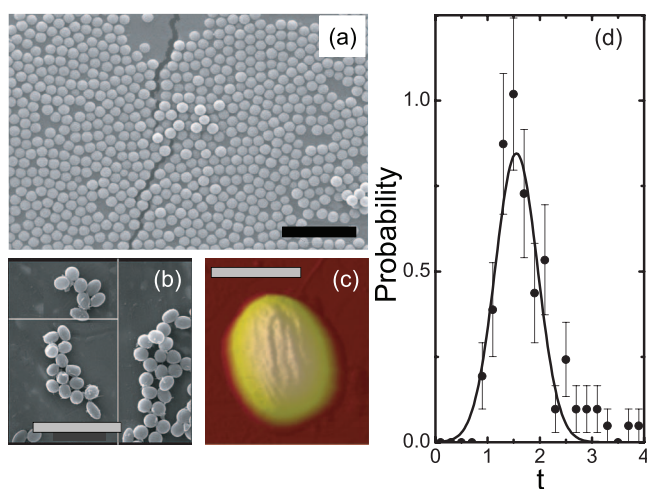

FIG. 1. (a) SEM image of the original colloidal spheres demonstrates that their polydispersity is very low. (b) SEM image of the prolate ellipsoids, obtained by stretching; the particles are oriented at different angles to the substrate, so that the apparent aspect ratios are smaller than their actual aspect ratio t. (c) 3D reconstruction of one of the ellipsoidal particles based on AFM (atomic force microscopy) measurement. (d) The ellipsoid aspect ratio distribution obtained from the SEM images (described in the text); the peak is at $t = 1.55 \pm 0.06$. This distribution was obtained from our SEM images, using the high uniformity of the initial spheres [see (a)] to extract the inclination of the spheroids with respect to the substrate; see details in the text. The scale bar length is 15 μm in (a) and (b) and 2 μm in (c).

obtained by the stretching procedure (see the Appendix), are shown in Fig. 1(b).

In addition, we measure the 3D shape of our ellipsoids, deposited on an aluminum surface, employing an AFM. The resulting images, such as in Fig. 1(c) allow, in principle, the full shape of the particle to be characterized, regardless of the inclination angle of the particle with respect to the substrate. Unfortunately, the AFM scanning speed is too low. Thus, to collect sufficient statistics for shape characterization, we employ faster two-dimensional SEM measurements.

We use our SEM images, such as in Fig. 1(b) to measure the distribution of the aspect ratios of our ellipsoidal colloids. Particle inclination angles, with respect to the (roughly) horizontal substrate, make them appear shorter in SEM images. Fortunately, the volumes of our ellipsoids, obtained by volume-conserving stretching of monodisperse spheres, are almost perfectly monodisperse [see Fig. 1(a)]. Moreover, our particles are spheroids, such that they are symmetric under rotation about their long axis. Therefore, the minor axis of a particle b can be measured quite accurately by SEM, being independent of the inclination angle of the particle with respect to the substrate. We obtain the aspect ratio and the inclination angle of each individual particle in our SEM images, based on the known volume of the initial spheres ($v = 7.24$ μm^3) and the minor axis length of the given particle, measured from the SEM image. The distribution $P(t)$ of the resulting aspect ratios $t = 6v\pi^{-1}b^{-3}$, based on ~100 SEM images of colloidal particles, is shown in solid symbols in Fig. 1(d); the symbols represent binned probabilities, with their integral normalized to unity. A Gaussian fit to our experimental distribution peaks at $t = 1.55 \pm 0.06$ and the median of our experimental data is $t = 1.6$. Both of these values are in perfect agreement with the nominal aspect ratio of our ellipsoids $t = 1.6$, confirming the accuracy of our stretching protocol. The width of the $P(t)$ distribution (HWHM = 0.47) is non-negligible. While the imperfect monodispersity of particle aspect ratios does not significantly change the structure of our fluids, as detailed in the following, it may significantly impact crystal stability and crystallization kinetics[38] in this system. We suggest that our protocol for characterization of aspect ratio distributions in colloidal spheroids should be adopted in a wide range of future studies employing these systems.

C. Preparation of the colloidal suspension

To thermalize our particles, we suspend them in a mixture (18:22:60, by mass) of cis-decahydronaphthalene (Fluka, 98%), tetrahydronaphthalene (Sigma-Aldrich, 99%), and tetrachloroethylene (Sigma-Aldrich, 99.5%). This mixture matches the refractive index of our particles. The gravimetric density of this mixture is slightly lower than that of our colloids, such that the sedimentation is balanced by the osmotic pressure.[39] As a result, a colloid density profile is formed within the sample. This profile stays unchanged on a scale of several weeks, indicating that the thermodynamical equilibrium was attained.

The preparation process of our ellipsoids damages parts of the steric PHSA layer.[24] To stabilize our particles by

short-ranged screened Coulombic repulsions,[40] we introduce 70 mM aerosol OT (AOT, or dioctyl sodium sulfosuccinate, Sigma-Aldrich, 98%) to the suspension. At very small concentrations, the AOT micelles charge the particles. At larger concentrations, the micelles screen Coulombic interactions, decreasing the range of Coulombic repulsions between the particles. The Debye length in our solvent, in absence of colloids, was previously estimated[41] as ~0.3 μm. This charging may in principle increase the effective size of a colloidal particle beyond its geometrical size, which is common in colloidal suspensions.[42] In order to approximate this effect in the theoretical model mentioned in Sec. IV B, we can rescale the theoretical ellipsoids by adding a distance wb to both of their axes. The aspect ratio of the effective particles will then become $t' = (w + t)/(w + 1)$. The volume fraction of these effective particles will become $\phi' = \phi(t'/t)(1 + w)^3$.

D. Confocal measurements and image analysis

For confocal imaging, the sample is loaded into a Vitrocom capillary ($0.1 \times 2 \times 50$ mm) and sealed with an epoxy glue. Our resonant laser scanning confocal setup Nikon A1R is capable of obtaining 512×512 pixel images at a rate of 30 frame/s, which is close to the video rate. For rapid acquisition of 3D stacks of confocal slices through the sample, we mount our objective on a piezo-z stage, such that a collection of 100 slices, separated by 0.3 μm takes only several seconds. At this high data acquisition rate, the diffusion of particles, even for the low density samples, does not matter for structure determination. The images are taken with an oil-immersed 100x Plan Apo objective. The lateral digital resolution is set to 0.08 μm/pixel, which slightly oversamples beyond the optical resolution of our setup. This oversampling improves the accuracy of our particle tracking procedures.[18,19]

We used particle tracking codes[43] based on the PLuTARC implementation[18] of the Crocker and Grier algorithm[19] for tracking simple spheres. We have generalized the code to track ellipsoids. The first part of the code analyzes each individual two-dimensional confocal slice. A slice through an ellipsoidal particle is an ellipse. The code detects the centers and orientational angles of all such ellipses, in each of the slices. The second part of the code links the centers of ellipses belonging to different slices, based on the lateral separation and orientation. The reconstructed particle positions are rendered in 3D in Fig. 2(a).

To determine the local volume, available for each particle, we perform a Voronoi tessellation of the reconstructed samples. The Voronoi cell of a given particle is the locus of all points, which are located closer to the center of this particle, than to any other particle in the system. The tesselation is carried out using the free Qhull software.[44] To estimate the local volume fraction ϕ of the colloids we divide the single-particle volume $v = \pi b^3 t/6$ by the volume of its Voronoi cell. The osmotic colloid density profile in our samples $\phi(z)$, discussed elsewhere,[1] is then obtained directly from the average ϕ values, measured at different elevations from the bottom of the sample. This makes it possible to measure, within each individual sample, the structure at different elevations from
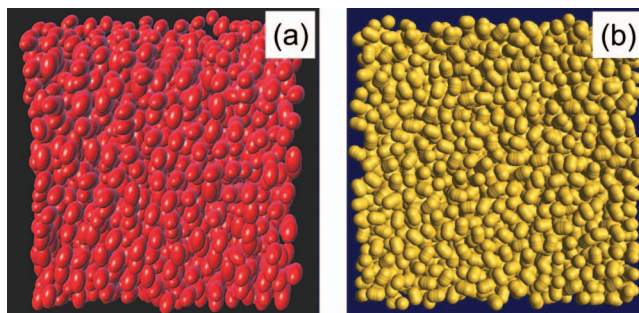

FIG. 2. (a) 3D reconstruction of the experimental particle positions, obtained by confocal microscopy at a volume fraction of $\phi = 0.26$. (b) 3D rendering of a system of L_3 particles, whose shapes closely approximate the experimental ellipsoids at $\phi = 0.26$.

the bottom of the capillary. Each of these elevations corresponds to a slightly different volume fraction, such that a large amount of information is obtained from each individual sample. The $\phi = 0.31$ data were obtained from a slab of thickness $9b$, over which $\phi(z)$ varied between 0.310 and 0.314; the $\phi = 0.26$ data were obtained from a $10b$-thick slab, where $\phi(z)$ ranged from 0.23 to 0.28. The similar outcomes for the two values of ϕ indicate that the variation in $\phi(z)$ does not significantly affect the results.

III. RESULTS

We quantify the local structure of the fluid of prolate ellipsoids by means of the radial distribution function[30] $g(r)$, which is proportional to the probability of finding two particles with their centers separated by a distance r. $g(r)$ is normalized so that it equals to 1 for an ideal gas. Our particles do not interpenetrate; thus $g(r) = 0$ for $r < b$, as demonstrated in Fig. 3, for two different particle volume fractions, $\phi = 0.26$ and $\phi = 0.31$. The peaks of $g(r)$ correspond to the coordination shells surrounding each particle in the fluid. Fluids are characterized by short-range positional correlations, and $g(r \to \infty) = 1$, as in the ideal gas. The rotational anisotropy of our ellipsoids may be expected to smear the shell structure of the fluid. However, in Fig. 3(b) the 3rd and the 4th coordination shells are visible, indicating the presence of positional correlations that increase with ϕ, as in simple fluids.[30]

A. Hard potential: Percus-Yevick approximation

To gain a deeper quantitative understanding of the experimental $g(r)$ data we compare the results to theoretical predictions based on the well-known Percus-Yevick (PY) approximation.[30] The PY model introduces an approximate closure to obtain an analytical solution for the Ornstein-Zernike (OZ) equation, which reproduces the experimental $g(r)$ of simple colloidal hard spheres.[10] Extension of the PY approximation to ellipsoids has been carried out numerically by Letz and Latz.[45] The pair potential of hard ellipsoids depends, in a complex way, on their separation and orientation; to overcome this difficulty, the well-known Berne-Pechukas approximation[46] was used, modified to describe hard interactions.[45] The solution of the OZ equation[47] yields
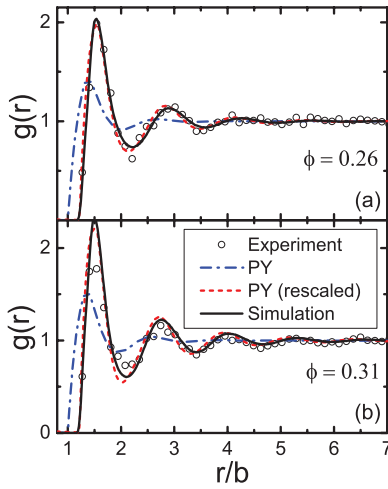
FIG. 3. Experimental[1] (dots), PY-theoretical[1,45] (dashed-dotted lines), and simulated (solid lines) radial distribution functions $g(r)$ for (a) $\phi = 0.26$ and (b) $\phi = 0.31$. The r values are normalized by the ellipsoid minor axis b, as measured by SEM. To improve the quality of the agreement, the PY-theoretical ellipsoids are rescaled by adding $wb = 0.22b = 0.46$ μm to both of their axes; such rescaling may be justified by Coulomb effects (see Sec. IV B). The resulting $g(r)$ (dashed lines), where ϕ and t were adjusted accordingly, exhibit much better agreement with the experiment.

$g(r)$ and the structure factor $S(q)$, which is related[30] to the Fourier transform of $g(r)$. The calculated $S(q)$ were only recently compared with event-driven molecular dynamics simulations of hard ellipsoids, for several different combinations of t and ϕ;[48] the results showed agreement between the analytical and the simulated $S(q)$. The comparison of the PY-based $g(r)$ with our experimental data is much less encouraging, as shown in Fig. 3; the PY $g(r)$ significantly underestimates positional correlations, with the oscillations in $g(r)$ decaying much faster than observed experimentally.[1] Importantly, this disagreement with experiment is not related to the finite shape polydispersity of the colloids [Fig. 1(d)]; indeed, introducing shape polydispersity into the theory further suppresses positional correlations,[49] resulting in even larger deviations from experiment.

B. Molecular dynamics simulations

In order to determine whether the discrepancy between the experimental results and PY theory is due to the inadequacy of the theory we have carried out molecular dynamics (MD) simulations[29] of systems of particles whose shapes approximate the colloidal ellipsoids. The particles consist of rigid assemblies of overlapping identical soft spheres positioned to reproduce the required shape. The interactions between particles are determined by combining the individual interactions of those pairs of soft spheres whose separation r is less than the cutoff range r_c; the interaction is the repulsive truncated LJ (Lennard-Jones) potential[29]

$$u_{ss}(r) = \begin{cases} 4\epsilon[(\sigma/r)^{12} - (\sigma/r)^6 + 1/4] & r < r_c = 2^{1/6}\sigma \\ 0 & r \geq r_c \end{cases}.$$

(1)

The parameters σ and ϵ can be used to define convenient MD length and energy units, respectively, with mass expressed in
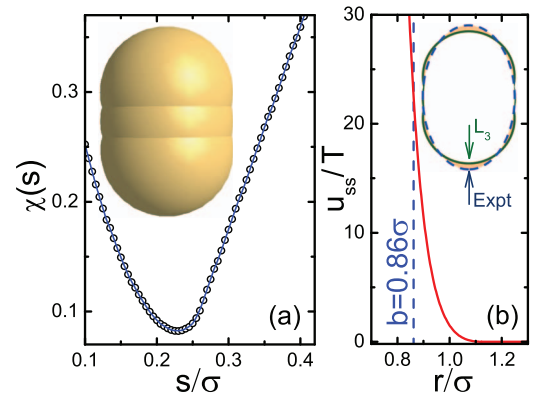

FIG. 4. (a) Fitting the shape of an L_3 particle to match the experimental ellipsoids by tuning the separation between the spheres of L_3. The longitudinal cross sections are overlayed in (b), where the non-overlapping area is shaded. χ is the ratio between the non-overlapping and overlapping area. With the soft sphere 'geometrical' diameter set to 0.86σ (see text), minimal χ is at $s \approx 0.22\sigma$ [this is the value used for the cross sections shown in (b)]. The interaction potential between the spheres of L_3 appears in (b); the vertical dashed line corresponds to the fitted value of the "geometrical" diameter of these spheres (see discussion in Sec. IV A).

terms of the sphere mass, and the MD temperature unit T obtained by setting $k_B = 1$.

Our approach, where the ellipsoids consist of rigid assemblies of soft spheres, is readily extended to other particle shapes and potentials. An alternative approach for ellipsoidal particles involves the use of anisotropic hard particles[48] or interaction potentials;[46] this method lacks both the computational simplicity of the present approach and its extensibility to particles of arbitrary shape.[50,51] Comparison of published computational results to the experimental data is not possible because of the different parameter values used in these studies.[48,52,53]

In the present work, we use a sphere assembly labelled "L_3," which is a linear array of three overlapping spheres with spacing $s < \sigma$ chosen to approximate the shape of the colloidal ellipsoids, as shown in Fig. 4. [The shape shown in Fig. 4(b) also corresponds closely to an equipotential.]

The simulations involve systems of 8000 particles, run at $T = 0.67$, for which the mean translational kinetic energy is unity [see Fig. 2(b)]. Periodic boundaries are used and the simulation cell size is determined by the overall number density. It should be pointed out that the MD approach is used here only to sample equilibrium configurations; the dynamics is not that of a colloidal system since the solvent is absent.

C. Simulation results for "L_3" particles

To compare the simulated $g(r)$ with experiment, the value of b (the short axis of the experimental ellipsoidal colloids) must be related to σ, which sets the length scale for the computer simulations. The experimental b as obtained from SEM images does not necessarily reflect the range of interparticle interactions; in particular, if Coulombic repulsions are present (see Sec. II C), the distance of closest approach between colloids is increased beyond their geometrical size. To have the position of the principal peak of the simulated $g(r)$ match the experimental data we set $b = 0.86\sigma$. In the following,

we refer to b as the "geometrical minor axis" of L_3, which (as with the experimental colloids) does not necessarily match the distance of closest approach of the centers of mass. As evident from the shape of the L_3 assembly [in the inset to Fig. 4(a)], b also defines the "geometrical diameter" of the soft spheres, which constitute this assembly. Once the b value is set, we fit the spacing s between the spheres to optimize the match between the shape of L_3 and that of the experimental ellipsoids, as shown in the inset to Fig. 4(b). The optimal match is obtained for $s = 0.22\sigma$, and the cross section of the resulting L_3 closely matches the shape of the experimental ellipsoids (see Fig. 4).

Fixing s and b determines the volume of L_3 as $v = \pi b^3 [1 + 3(s/b) - (s/b)^3]/6$. For a given experimental colloidal volume fraction ϕ, the number density of the simulation is set to ϕ/v. Figure 3 shows the simulated $g(r)$ curves for two different ϕ, and these are seen to be in very good agreement with experiment. This suggests that finite shape polydispersity of the experimental colloids [Fig. 1(d)] does not significantly change the structure of our colloidal suspensions.

IV. DISCUSSION

A. Estimating interparticle potential

The good agreement of the L_3 simulations with the experimental $g(r)$, with only one adjustable parameter used for both ϕ values, suggests that simply rescaling particle size captures the most important properties of the experimental system. This fact can be used to gain a deeper insight into the actual interaction between the colloids. The fitted $b = 0.86\sigma$ is close to the distance of closest approach in a simple soft sphere system, which, by examination[29] of $g(r)$ is 0.9σ. With b identified as the minor axis of the colloidal particle [vertical dashed line in Fig. 4(b)], the contribution $u_{ss}(r > b)$ produces a similar effect to that of the screened Coulombic interactions due to the presence of AOT micelles in the experimental system. To gain a more quantitative insight into the nature of colloidal interactions in the system, we calculate the second virial coefficient of the simulated soft spheres,

$$B_2 = -2\pi \int_0^\infty [exp\,(-u_{ss}(r)/k_B T) - 1] r^2 dr$$
$$= 2.3\sigma^3 = 3.6 b^3. \qquad (2)$$

The exact shape of the simulated $u_{ss}(r)$ may not be an accurate representation of the experimental interaction potential. However, the good match between the simulated $g(r)$ and experiment suggests that at least the B_2 values, corresponding to the largest term in the virial expansion, should be correct. For an experimental charged spherical particle of size b, the B_2 coefficient can be separated in two parts: (a) the second virial coefficient due to the short-ranged hard potential of the particle $B_2^{HS} = 2\pi b^3/3$; (b) a contribution due to the screened Coulombic interactions $B_2^{DL} = B_2 - B_2^{HS}$. In particular, if B_2 of a colloidal sphere of size b is the same as in the simulations, we get $B_2^{DL} = 1.5 b^3$. To account for the Coulombic interaction, we adopt the classical formalism of Verwey and Overbeek,[40] which is widely used with various aqueous suspensions. According to this formalism, the interaction poten-

tial between two charged colloidal spheres, due to the overlap of their electrical double layers, is

$$V_{DL}(r) = \pi \epsilon_0 \epsilon_r \sigma \psi_0^2 ln \left\{ 1 + exp \left[-\kappa \sigma \left(r/\sigma - 1 \right) \right] \right\}, \qquad (3)$$

where $\epsilon_r \approx 2.5$ is the dielectric constant of the medium and

$$\psi_0 = (\pi \epsilon_0 \epsilon_r \sigma)^{-1} Q_s/(2 + \kappa\sigma) \qquad (4)$$

is the surface potential of the sphere, carrying an electrical charge Q_s. While the exact expressions for the interaction potentials of the ellipsoids are complicated,[54,55] the sphere assemblies used in our simulations provide an approximation for these anisotropic interactions. The corresponding contribution to the second virial coefficient is then given by

$$B_2^{DL} = -2\pi \int_\sigma^\infty [exp(-V_{DL}(r)/k_B T) - 1] r^2 dr. \qquad (5)$$

With the Debye length in the solvent estimated as $\kappa^{-1} = 300$ nm (Sec. II C), a charge of $Q_s \approx 60e$ must be present on the surface of a colloidal sphere, to obtain $B_2^{DL} = 1.5 b^3$, which accounts for the extra repulsion between the simulated spheres. Thus, we estimate the equivalent dimensionless charge[41,56,57] of the experimental ellipsoids as $Z\lambda_B/R$, where $R = \sigma_s/2$ is the radius of the initial spherical colloids before stretching, $\lambda_B = e^2/(4\pi\epsilon_0\epsilon_r k_B T) \approx 23$ nm is the Bjerrum length[40] and $Z = 3Q_s/e$ is the valency of an experimental colloid, which is here approximated by an assembly of three soft spheres. The resulting value of this simplistic calculation $Z\lambda_B/R \approx 3$ agrees with $Z\lambda_B/R = 2.6$ obtained for an apolar system of spherical colloids by direct measurements of the electric charge.[41,56,57] This charge, which is very small compared to the typical electrical charges in an aqueous colloidal dispersion ($\epsilon_r \sim 80$), cannot be neglected in our apolar system ($\epsilon_r \approx 2.5$).

B. Rescaled PY approximation

Charging effects were not taken into account in the PY model of hard ellipsoids (Sec. III A). Thus, the poor agreement between PY and experiment (Fig. 3) is hardly surprising. In order to account for Coulomb effects, the theoretical hard ellipsoids must be rescaled, as described in Sec. II C. Thus, we add a distance wb to both the major and minor axes of the particles, where w is a free adjustable parameter. The aspect ratio and the volume fraction of the ellipsoids are then adjusted accordingly (see Sec. II C). The best match between the PY model and experiment occurs for $w = 0.22$. This results in a major improvement compared to the original PY analysis, as shown in Fig. 3. The fitted increase in the radius of the particles $wb/2 \approx 230$ nm is close to the estimated thickness of the double layer in our system being equal to 300 nm (see Sec. II C).

The rescaled version of PY model provides an independent test of the interparticle potentials obtained in Sec. IV A. The second virial coefficient of a hard spheroid is $B_2^{HE} = v + RS$, where R, S, and v are the mean radius of curvature, surface area, and volume of the particle.[58] In particular, if the minor axis is b and the aspect ratio is $t = 1.6$, we obtain $B_2^{HE} = 3.6 b^3$. The rescaled spheroid,

with a minor axis of $1.22b$ and an aspect ratio of 1.49, yields $B_2^{SE} = 5.9b^3$. Therefore, the double layer contribution to the second virial coefficient is $B_2^{SE} - B_2^{HE} = 2.3b^3$. A ~1.5-fold smaller value was calculated in Sec. IV A for $B_2^{DL} = 1.5b^3$, which is the double layer contribution to B_2 for each of the spheres in the L_3 assembly. This can be justified by noting that the spheres in the L_3 assembly have only part of their surface exposed to the surrounding fluid; the unexposed parts of the surface do not contribute to B_2. Approximating the L_3 by an ellipsoid, we estimate the exposed area of an L_3 assembly to be larger by a factor of ~1.4, compared to that of a sphere of diameter b. Therefore, we estimate the charge contribution to B_2 of the spheres to be smaller by roughly the same factor: $2.3b^3/1.4 \approx 1.6b^3$, very close to the value which was calculated in Sec. IV A. This further supports the conclusion that charge effects play a significant role in determining the structure of these colloidal fluids.

V. CONCLUSIONS

We have studied the structure of a fluid of colloidal ellipsoids. The shape polydispersity of these ellipsoids has been characterized, employing a new protocol based on SEM measurements. We have demonstrated that the structure of the colloidal fluid can be reproduced by molecular dynamics simulation, employing L₃ particles to approximate the shape of the experimental ellipsoids. These simulations allow the charge effects in the experimental system to be estimated, with the charge per particle reaching ~$200e$, a non-negligible charge for an apolar colloidal suspension. Equivalent results can be obtained from a similarly rescaled PY calculation.

These results demonstrate that important insights into the physics of these fundamental fluids can be achieved by a combination of experiment and computer simulation. In the future, we plan to study the combined orientational and positional correlation functions, to determine their mutual interdependence. We anticipate that future efforts in this direction should provide a deeper understanding of the bulk and surface phases which are formed in these simple but fundamental systems.

APPENDIX: STRETCHING OF COLLOIDAL SPHERES

To stretch our colloidal spheres,[21] we suspend them in a 25% (w/w) solution of hydroxy terminated PDMS (typ-ical molecular weight $M_n = 10^5$, Sigma-Aldrich) in hexane (BioLab, AR >96%). The volume fraction of spheres in this mixture is low, $\phi \approx 0.03$. Next, a cross-linking agent, trimethylsilyl terminated poly(dimethylsiloxane-co-methylhydrosiloxane) ($M_n = 950$, Sigma-Aldrich) and a catalyst [tin(II) 2-ethylhexanoate, Sigma-Aldrich, ~95%] are added to polymerize the PDMS, to form a rubber matrix. The weight fractions of the cross-linking agent and the catalyst are 6×10^{-3} and 8×10^{-3}, respectively. Immediately after the introduction of the cross-linking agent and the catalyst, the suspension is poured onto a rectangular mold, where ~1 mm-thick composite rubber film forms. When the cross-linking reaction is over (~13 h later), the films are post-cured for 2 h in an oven, pre-heated to 120 °C. The rubber is then uniaxially stretched to a desired length inside an oven, at $T = 180$ °C, above the glass transition temperature of the colloids. In order to make the stretching process accurate and reproducible, to minimize film tearing, and to reduce the shape polydispersity of the resulting ellipsoids, we have constructed a computerized stretching device. This device, mounted inside the oven, is capable of stretching the films at sufficiently slow and uniform rates, <70 μm/s. The door of our oven is equipped with a glass window, which allows the stretching process to be followed visually in real time. Assuming that the volume of an individual particle is conserved in our uniaxial stretching process, the aspect ratio of the particle t is related to the elongation Δl of the film as $t = (1 + \Delta l/l)^{3/2}$, where l is the initial length of the film. Thus, to obtain ellipsoids which have an aspect ratio of $t = 1.6$, we stretch the film by 37% of its length $l \approx 3$ cm. After the stretching, the oven is cooled down to the ambient temperature and the film is removed from the stretching device.

We release the ellipsoids by destroying the PDMS matrix. The PDMS films are first swollen in hexane for 24 h. Then, the films are transferred to a mixture of iso-propyl alcohol (Frutarom, AR) and hexane (5:23 w/w), to which a small amount (0.04%, w/w) of sodium methoxide (Fluka, >97%) is added. This mixture is filled into an hermetically sealed flask, which is placed on a magnetic stirring plate. To have the film cut into many small fragments, each of which is readily destroyed by sodium methoxide, we put a piece of a ferromagnetic razor into the flask, instead of a common Teflon-coated magnetic stirrer. The razor is agitated by the magnetic field of the stirring plate, cutting the PDMS film and mixing the solution. When the film is fully degraded, the particles are sedimented by centrifugation and transferred to mixed decahydronaphthalene (mix-DHN, Sigma-Aldrich, 98%) or hexane.

[1]A. P. Cohen, E. Janai, E. Mogilko, A. B. Schofield, and E. Sloutskin, Phys. Rev. Lett. **107**, 238301 (2011).

[2]S. F. Schulz, E. E. Maier, and R. Weber, J. Chem. Phys. **90**, 7 (1989).

[3]Z. Dogic and S. Fraden, *Soft Matter: Complex Colloidal Suspensions*, edited by G. Gompper and M. Shick (Wiley-VCH, Weinheim, Germany, 2005), Chap. 2.

[4]P. Levitz, M. Zinsmeister, P. Davidson, D. Constantin, and O. Poncelet, Phys. Rev. E **78**, 030102 (2008).

[5]E. Belamie, P. Davidson, and M. M. Giraud-Guille, J. Phys. Chem. B **108**, 14991 (2004).

[6]M. P. B. van Bruggen, H. N. W. Lekkerkerker, and J. K. G. Dhont, Phys. Rev. E **56**, 4394 (1997).

[7]G. J. Vroege and H. N. W. Lekkerkerker, Rep. Prog. Phys. **55**, 1241 (1992).

[8]V. J. Anderson and H. N. W. Lekkerkerker, Nature (London) **416**, 811 (2002).

[9]R. P. A. Dullens, Soft Matter **2**, 805 (2006).

[10]R. P. A. Dullens, D. G. A. L. Aarts, and W. K. Kegel, Proc. Natl. Acad. Sci. U.S.A. **103**, 529 (2006).

[11]A. Yethiraj and A. van Blaaderen, Nature (London) **421**, 513 (2003).

[12]R. M. Erb, R. Libanori, N. Rothfuchs, and A. R. Studart, Science **335**, 199 (2012).

[13]P. J. Lu, E. Zaccarelli, F. Ciulla, A. B. Schofield, F. Sciortino, and D. A. Weitz, Nature (London) **453**, 499 (2008).

[14]J. Mattsson, H. M. Wyss, A. Fernandez-Nieves, K. Miyazaki, Z. Hu, D. R. Reichman, and D. A. Weitz, Nature (London) **462**, 83 (2009).

[15]G. Bosma, C. Pathmamanoharan, E. H. A. de Hoog, W. K. Kegel, A. van Blaaderen, and H. N. W. Lekkerkerker, J. Colloid Interface Sci. **245**, 292 (2002).

[16]P. J. Lu, Ph.D. dissertation (Harvard University, 2008).

[17]E. R. Weeks, "Microscopy of soft materials," in *Experimental and Computational Methods in Soft Condensed Matter*, edited by J. S. Olafsen (Cambridge University Press, Cambridge, England, 2010).

[18]P. J. Lu, P. A. Sims, H. Oki, J. B. Macarthur, and D. A. Weitz, Opt. Express **15**, 8702 (2007).

[19]J. C. Crocker and D. G. Grier, J. Colloid Interface Sci. **179**, 298 (1996).

[20]D. T. Valley, S. A. Rice, B. Cui, H. M. Ho, H. Diamant, and B. Lin, J. Chem. Phys. **126**, 134908 (2007).

[21]A. Mohraz and M. J. Solomon, Langmuir **21**, 5298 (2005).

[22]D. Mukhija and M. J. Solomon, Soft Matter **7**, 540 (2011).

[23]Z. Zheng, F. Wang, and Y. Han, Phys. Rev. Lett. **107**, 65702 (2011).

[24]Z. Zhang, P. Pfleiderer, A. B. Schofield, C. Clasen, and J. Vermant, J. Am. Chem. Soc. **133**, 392 (2011).

[25]E. B. Mock and C. F. Zukoski, Langmuir **23**, 8760 (2007).

[26]C. Baravian, L. J. Michot, E. Paineau, I. Bihannic, P. Davidson, M. Impéror-Clerc, E. Belamie, and P. Levitz, Europhys. Lett. **90**, 36005 (2010).

[27]Z. Zheng and Y. Han, J. Chem. Phys. **133**, 124509 (2010).

[28]A. Kuijk, A. van Blaaderen, and A. Imhof, J. Am. Chem. Soc. **133**, 2346 (2011).

[29]D. C. Rapaport, *The Art of Molecular Dynamics Simulation*, 2nd ed. (Cambridge University Press, Cambridge, England, 2004).

[30]L. E. Reichl, *A Modern Course in Statistical Physics* (Wiley, 1998).

[31]Y. Han, A. M. Alsayed, M. Nobili, J. Zhang, T. C. Lubensky, and A. G. Yodh, Science **314**, 626 (2006).

[32]P. J. Yunker, T. Still, M. A. Lohr, and A. G. Yodh, Nature (London) **476**, 308 (2011).

[33]C. C. Ho, A. Keller, J. A. Odell, and R. H. Ottewill, Colloid Polym. Sci. **271**, 469 (1993).

[34]G. Bryant, S. R. Williams, L. Qian, I. K. Snook, E. Perez, and F. Pincet, Phys. Rev. E **66**, 060501(R) (2002).

[35]S. M. Underwood, J. R. Taylor, and W. van Megen, Langmuir **10**, 3550 (1994).

[36]Y. Lu, Y. Yin, Z.-Y. Li, and Y. Xia, Langmuir **18**, 7722 (2002).

[37]B. Frisken, Appl. Opt. **40**, 4087 (2001).

[38]S. Iacopini, T. Palberg, and H. J. Schöpe, J. Chem. Phys. **130**, 084502 (2009).

[39]R. Piazza, T. Bellini, and V. Degiorgio, Phys. Rev. Lett. **71**, 4267 (1993).

[40]R. J. Hunter, *Foundations of Colloid Science*, 2nd ed. (Oxford University Press, Oxford, UK, 2009).

[41]G. S. Roberts, R. Sanchez, R. Kemp, T. Wood, and P. Bartlett, Langmuir **24**, 6530 (2008).

[42]H. J. Schöpe, G. Bryant, and W. van Megen, Phys. Rev. Lett. **96**, 175701 (2006).

[43]A. P. Cohen, M.S. thesis (Bar-Ilan University, 2008).

[44]C. B. Barber, D. P. Dobkin, and H. Huhdanpaa, ACM Trans. Math. Softw. **22**, 469 (1996); see www.qhull.org.

[45]M. Letz and A. Latz, Phys. Rev. E **60**, 5865 (1999).

[46]B. J. Berne and P. Pechukas, J. Chem. Phys. **56**, 4213 (1999).

[47]Our solution follows exactly the original theoretical paper (Ref. 45), where the spherical harmonics series expansions were truncated after $L_{max} = 4$.

[48]C. De Michele, A. Scala, R. Schilling, and F. Sciortino, J. Chem. Phys. **124**, 104509 (2006).

[49]M. J. Pond, J. R. Errington, and T. M. Truskett, J. Chem. Phys. **135**, 124513 (2011).

[50]D. C. Rapaport, Phys. Rev. E **70**, 051905 (2004).

[51]D. C. Rapaport, Phys. Rev. Lett. **101**, 186101 (2008).

[52]J. Talbot, D. Kivelson, M. P. Allen, G. T. Evans, and D. Frenkel, J. Chem. Phys. **92**, 3048 (1990).

[53]D. Frenkel and B. M. Mulder, Mol. Phys. **55**, 1171 (1985).

[54]D. Chapot, L. Bocquet, and E. Trizac, J. Chem. Phys. **120**, 3969 (2004).

[55]C. Álvarez and G. Téllez, J. Chem. Phys. **133**, 144908 (2010).

[56]G. S. Roberts, T. A. Wood, W. J. Frith, and P. Bartlett, J. Chem. Phys. **126**, 194503 (2007).

[57]R. Kemp, R. Sanchez, K. J. Mutch, and P. Bartlett, Langmuir **26**, 6967 (2010).

[58]G. S. Singh and B. Kumar, J. Chem. Phys. **105**, 2429 (1996).